

Characterization of Magnetic Ni Clusters on Graphene Scaffold after High Vacuum Annealing

*Zhenjun Zhang, Akitomo Matsubayashi, Benjamin Grisafe, Ji Ung Lee, James R. Lloyd

College of Nanoscience and Engineering, SUNY Polytechnic Institute, Albany, NY 12203

Abstract

Magnetic Ni nanoclusters were synthesized by electron beam deposition utilizing CVD graphene as a scaffold. The subsequent clusters were subjected to high vacuum ($5-8 \times 10^{-7}$ torr) annealing between 300 and 600 °C. The chemical stability, optical and morphological changes were characterized by X-ray photoemission microscopy, Raman spectroscopy, atomic force microscopy and magnetic measurement. Under ambient exposure, nickel nanoparticles was observed to be oxidized quickly, forming antiferromagnetic nickel oxide. Here, we report that the majority of the oxidized nickel is in non-stoichiometric form and can be reduced under high vacuum at temperature as low as 300 °C. Importantly, the resulting annealed clusters are relatively stable and no further oxidation was detectable after three weeks of air exposure at room temperature.

Key words: metal, oxides, interfaces, electron beam-assisted deposition, X-ray photo-emission spectroscopy (XPS)

1. INTRODUCTION

Synthesis of nanometer scale metal clusters has attracted tremendous attention in recent years due to their unique properties, compared to the bulk counterparts [1]. These properties enable metal clusters to have possible applications in the area of biomedical drug

delivery, catalysis, imaging contrast enhancement and biochemical sensing [2-5]. Among all metal nanoclusters, magnetic metals such as nickel and cobalt are of particular interest. There is a wide range of reported methods to fabricate nickel or cobalt nanoclusters that can generally be classified in three different categories 1. Chemical reduction or decomposition 2. Physical vapor deposition. 3. Electrochemical deposition [6-10]. Graphene, a sp^2 hybridized carbon material, has already been widely studied for a variety of applications in electronics, spintronics and energy storage [11-13]. Hybridization of graphene with nanoclusters has shown potential in electrochemical devices and high performance catalysis [14, 15]. In addition, nanoclusters grown on graphene with low defect density can be used as thermal and electric carriers [16, 17]. Metal clusters on graphene sheets can be generated using wet chemistry but it has a tendency to sacrifice the conduction property of graphene. Due to lack of oxygen anchors, metals deposited on graphene tend to ball up and form clusters [18]. Using this property, it is possible to assemble metal decorated graphene on an arbitrary substrate.

To date, numerous reports have been focused on the study of well dispersed metal arrays on the CVD graphene moiré on close-packed metal surfaces. In these reports, high arrays of quality metal clusters such as (Re, W, Pt, Ir, Ni) can be synthesized in ultra-high vacuum using well controlled deposition techniques and highly ordered substrates [19-23]. However, fabrication of metal nanoclusters on transferred graphene with arbitrary substrates is not well studied. Furthermore, the stability of some of the oxophilic metals is not well characterized. Specifically, nickel thin films are vulnerable to oxidation at ambient condition and it is expected this effect can be worsened if the nickel is in the form of nanoclusters, in which large surface areas are in contact with the ambient environment.

When unprotected, nickel clusters are usually in a partially oxidized condition [24]. Partially oxidized nickel or cobalt nanoparticles are well known to exhibit hysteresis loops along the magnetic field axis, namely exchange bias (EB) [25, 26]. It happens when ferromagnetic components (nickel or cobalt) is exchange coupled with an antiferromagnetic component (nickel or cobalt oxide) at the interface. This property is useful not only in spintronic devices but also for probing the properties at the ferromagnetic-antiferromagnetic interface [27]. Very recently, cobalt oxide has been reported to be partially reduced at high vacuum annealing conditions and showed significant reduction of exchange bias afterwards [27].

Here we demonstrate a simple method to hybridize nickel nanoclusters with graphene on an arbitrary substrate, investigate the oxidation effects of electron beam deposited nickel nanoclusters on graphene under ambient exposure and study its change of properties after high vacuum annealing. Our XPS measurements show that the majority of the oxidized nickel is in nonstoichiometric form. We observed that nonstoichiometric nickel oxide can be reduced at temperatures as low as 300 °C under high vacuum annealing conditions. At 600 °C, nearly 95% of the oxide was transformed to the metallic form. Our magnetic measurements detect the hysteresis loop shift after ambient exposure but the exchange bias became symmetric after high temperature vacuum annealing, which is supplemental evidence for the reduction of nonstoichiometric nickel oxide.

2. EXPERIMENTAL

CVD graphene was used as the scaffold for the growth of nickel nanoclusters. The graphene was grown on a 25 micrometers thick commercially available polycrystalline Cu foil and was then dry transferred to a silicon substrate with 90 nm thermally grown SiO₂. To transfer graphene onto SiO₂, poly(methylmethacrylate) (PMMA) was coated onto as-grown CVD graphene on Cu foil and baked at 65 °C for 5 min to evaporate the solvent, followed by backside etching using a Technics 800 Micro RIE chamber with O₂ Plasma (30W, 30 Seconds). A thermal release tape was then attached to the PMMA film with a cut window in the center and floated on an ammonium persulfate solution (APS). After the copper residue was etched away and washed with de-ionized water, the graphene with PMMA support was transferred to a SiO₂ substrate. The PMMA layer was then removed in an acetone bath for 1 hr, followed by an isopropyl alcohol (IPA) rinse and dried in N₂ gas. The quality and layer of the as-transferred graphene sheet was monitored by Raman spectroscopy at 532 nm wavelength. The samples were then loaded into an electron beam evaporator chamber with a commercially available 99.9% pure nickel crucible and pumped down to a base pressure below 5×10^{-7} Torr. The nickel crucible was then locally heated by electron beam to reach the vaporizing pressure and deposited at a rate of 1Å/s for 30 second on two different substrates 1.nickel on graphene/SiO₂ 2.nickel on SiO₂. The samples are taken out of vacuum chamber and exposed to ambient air for 24h. The chemical state of the samples were characterized by both a Thermo Scientific Theta Probe XPS instrument and Verserlab Vibrating Sample Magnetometer (VSM). The morphology of the nickel nanoclusters was characterized with a Veeco Dimension 3100 AFM instrument.

After the initial characterization, the sample was loaded into a custom made vacuum chamber with a base pressure of 6×10^{-8} torr. After a quick temperature ramp that ranged

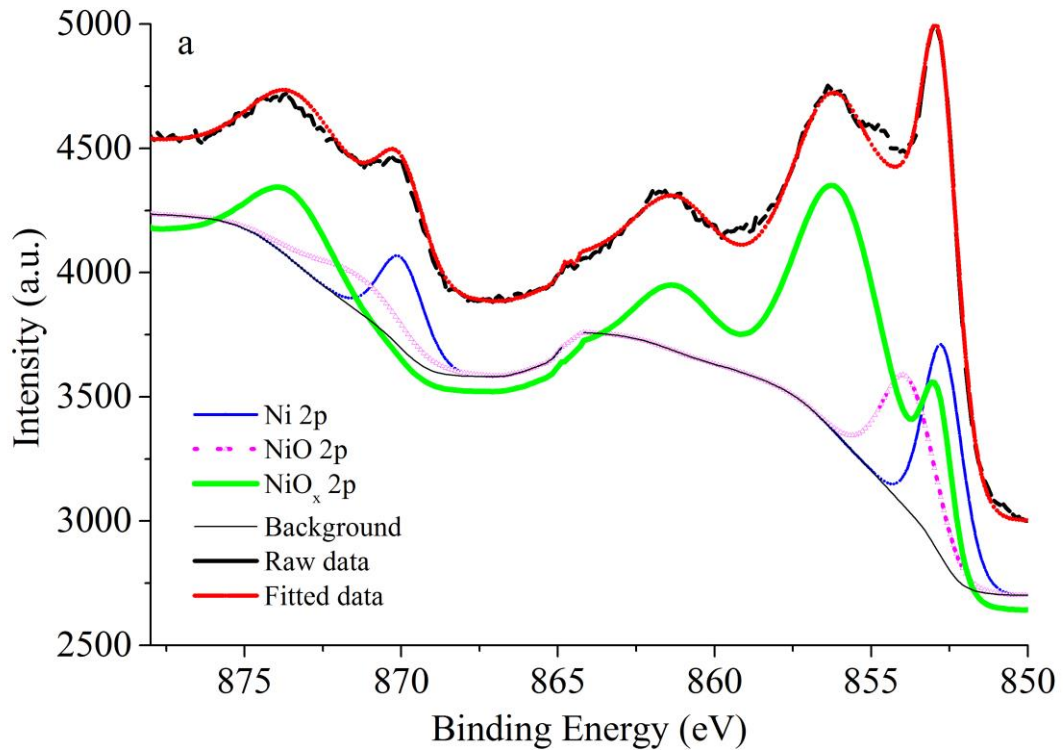
between 300 to 600 °C, the temperature was maintained for 1 hr, at a vacuum pressure between $5-8 \times 10^{-7}$ torr. The sample was then cooled down to room temperature by convection and further characterized with XPS and Verserlab VSM for comparison.

3. RESULTS AND DISCUSSION

Figure 1a and 1b shows the Ni 2p core emission XPS data after 24 hr air exposure and 1 hr high vacuum annealing (5×10^{-7} torr) at 300 °C. Because of the conductive nature of graphene, the sample under testing did not show a noticeable amount of charge shifting by measurement of the adventitious 1s carbon peak in the sample. In Figure 1a, the Ni 2p peak spectrum shows at least three distinct nickel species: (1) the metallic nickel (2) stoichiometric nickel oxide (3) $\text{NiO}_x \cdot y\text{H}_2\text{O}$. Taking account the spin-orbit splitting effect, the fitted peak at 852.7 and 853.8 eV correspond to the metallic nickel and NiO $2p_{3/2}$ binding energy, respectively. Another Ni $2p_{3/2}$ peak at 852.87 eV is assigned to a generic $\text{NiO}_x \cdot y\text{H}_2\text{O}$, due to the complication of multiplet splitting and plasmon loss effects for nickel 2p spectrum. To assure that the minor shift of the nickel 2p peak is not due to hybridization with graphene, a reference study was carried out on nickel deposited on SiO_2 and a similar result was obtained. Angle dependent XPS spectrum (not shown) confirmed that the nickel cluster is oxygen rich on the surface and nickel rich inside the core. The mechanism of oxidation effect on the as-deposited nickel nanoclusters is presumably related to its high surface to volume ratio and large oxygen concentration difference between that in equilibrium with a vacuum and ambient conditions. The as-deposited nickel clusters might have a high concentration of defects after e-beam evaporation. After ambient exposure, oxygen diffuses rapidly into the nickel cluster and occupies the defective sites to

form a non-stoichiometric oxide. In other words, the formation of non-stoichiometric oxide is kinetically driven and it is in metastable state at room temperature. After 1 hour of high vacuum annealing, the XPS spectrum of the sample became cleaner with less background noise, which is an indication of less roughness at the surface. The nickel $2p_{3/2}$ spectrum is fitted with a main peak at 852.7 eV and two broad satellite peak (FWHM 2.5 eV) with binding energy 856.4eV (minor), 858.7 eV (major) [28]. The disappearance of a major peak at 853.8 is attributed to the reduction of majority of the NiO_x . Rationally, this unusual reduction could be attributed to either direct dissociation of nickel oxide to the vacuum or reduction of nickel oxide with underlying substance. The standard free energy for nickel oxide to directly dissociate into metallic nickel and oxygen molecule is 187.3 kJmol^{-1} , which is energetically unfavorable. On the other hand, the standard free energy for carbon species to reduce nickel oxide into metallic nickel and carbon dioxide is -20.6 kJmol^{-1} (300°C). The questions comes to whether it is the graphene associated carbon involved in reduction. In parallel experiment for nickel/ SiO_2 showed similar results. It is reported that transition metal oxide can undergo reduction at temperature below 300°C in high vacuum condition (2×10^{-8} torr), assisted by surface carbon contaminants [29]. Therefore, small amount of surface carbon in our vacuum chamber can be the origin of reduction source. The accumulation of oxide at nickel surface and reduction was further evidenced by the $1s$ O peak in Figure 2. After ambient exposure, a significant amount of oxygen from nickel was detected. At 300°C in high vacuum annealing, the amount of oxide peak from nickel is dramatically reduced. After 600°C high vacuum anneal, the amount of oxygen in nickel clusters is further reduced to around 5% based on the normalized NiO_x $1s$ O peak intensity ratio in the XPS spectra. Even though the absolute value cannot be judged, the relative

amount of nickel oxide decreases to the minimum level at this temperature. Due to the fact that the whole measurement is performed ex situ, it cannot be ruled out that small amount oxidation may occur during the transfer process.



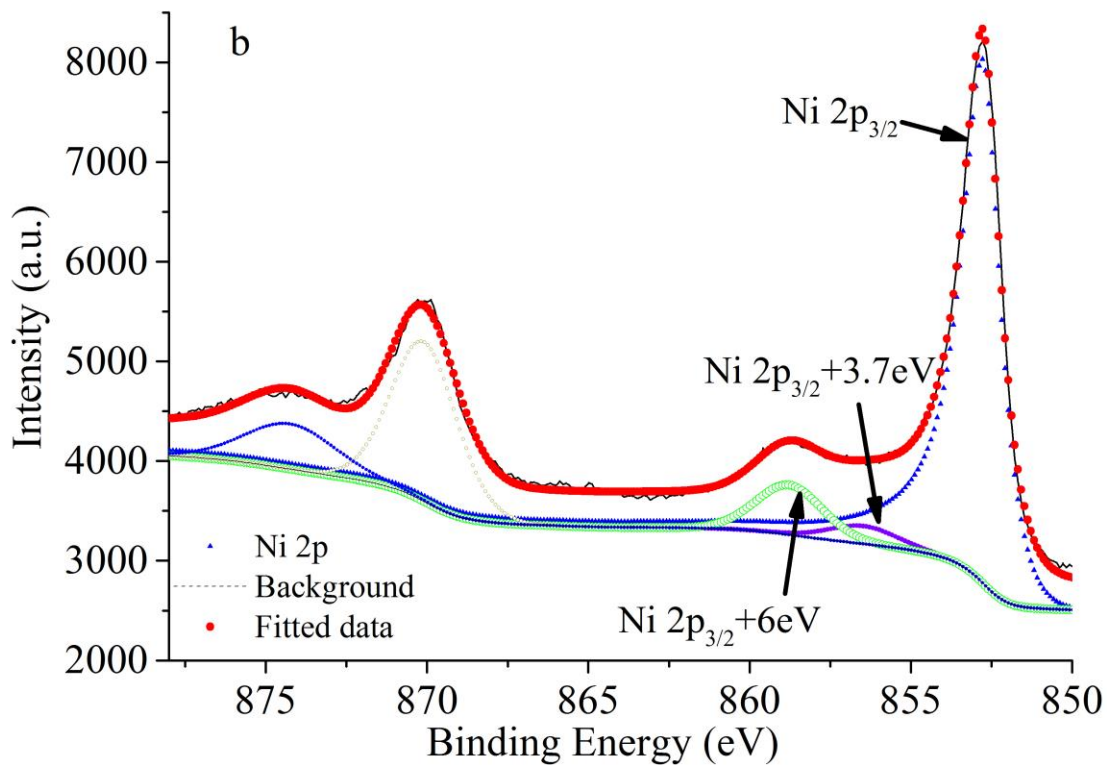


Figure 1. (Color online) Ni 2p X-ray photoelectron peaks: a) as-grown, b) 300 °C annealed.

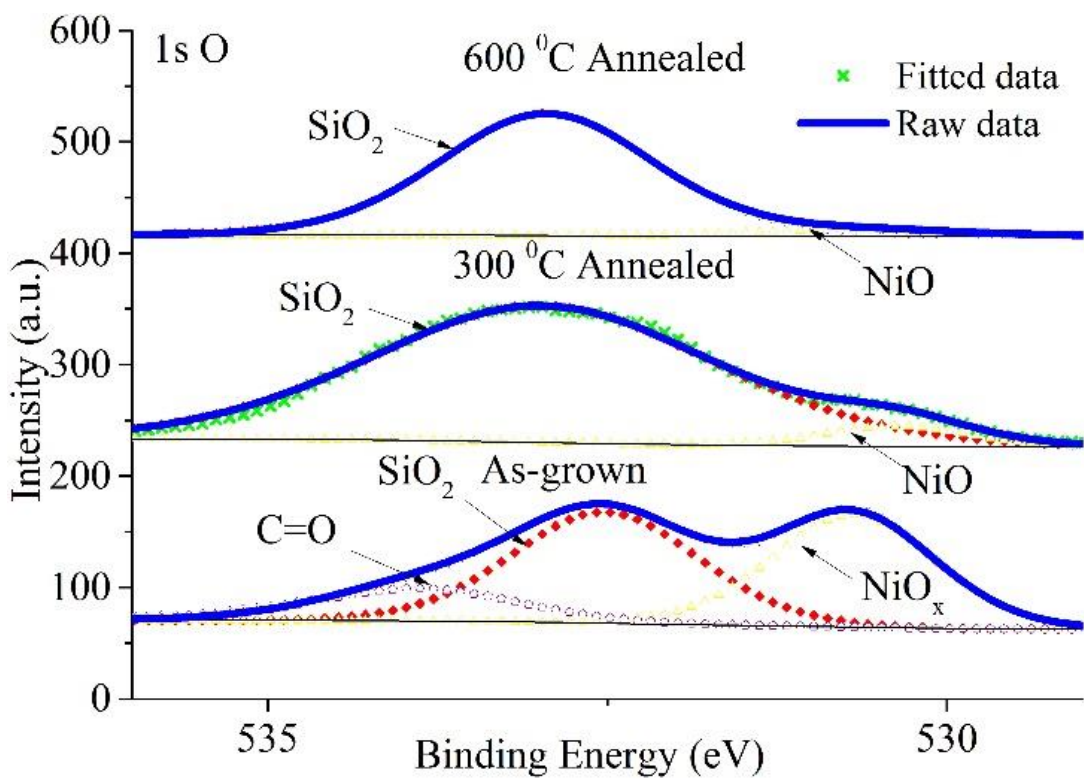


Figure 2. (Color online) Evolution of oxygen 1s X-ray photoelectron peaks: (1) as-grown, (2) 300^o C annealed, (3) 600^o C annealed.

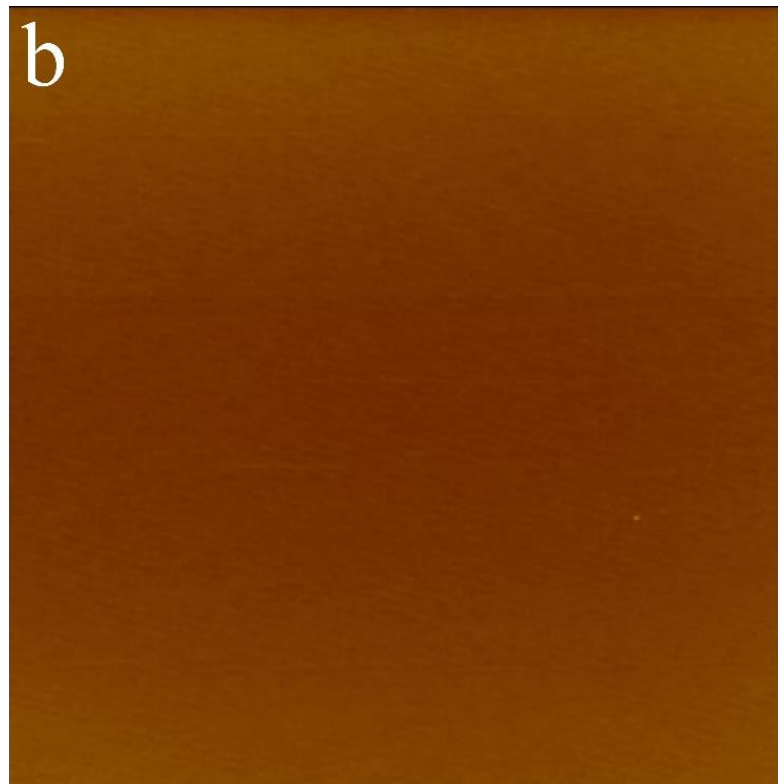
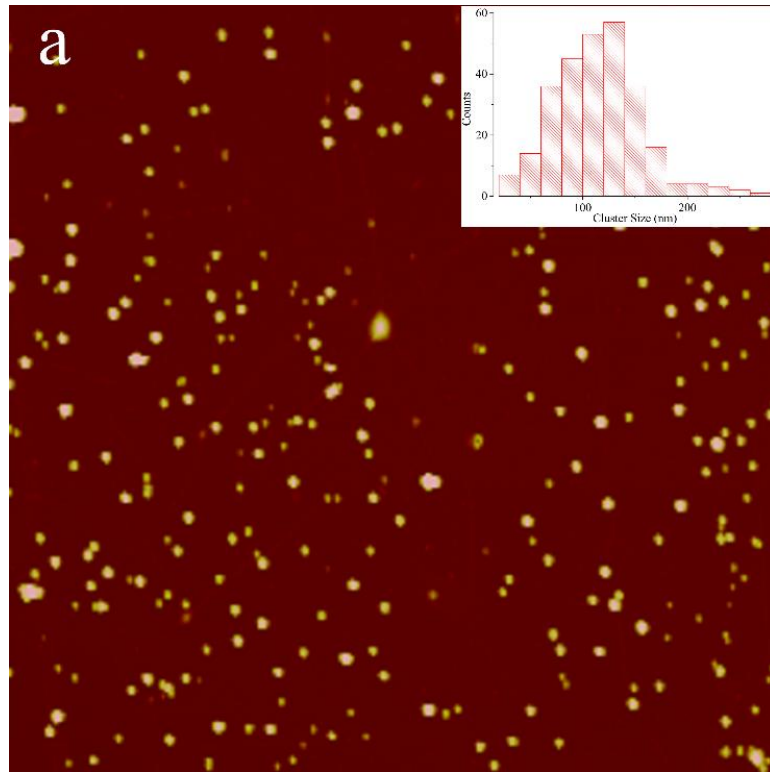


Figure 3. (Color online) AFM images (10x10 μm) of nickel sample on: a) graphene/SiO₂ with cluster size distribution on right side inset, b) SiO₂.

AFM was used to study the morphology of the nickel nanoclusters on graphene. Figure 3 shows the morphology of nickel on graphene. The average nanocluster size was around 123 nm (Figure 3a inset) with surface roughness (R_a) of 2.95 nm. The height of the nanoclusters ranged between 20 to 50 nm. In contrast, nickel on SiO₂ is rather uniform after deposition, with a mean average surface roughness of 0.46 nm. The dramatic difference can be explained by the surface free energy difference between graphene and SiO₂. The surface free energy of graphene is on the order of 46.7 mJ/m², which is 500 times smaller than nickel particles (2.45 J/m²) [30]. This suggests that metals will have sufficient mobility to migrate on graphene surface until reach to a high energy boundaries such as defective sites, resulting in cluster nucleation. In our case, the relative large cohesive energy (4.44 eV) for nickel favors the growth of the nanocluster in 3 D coverage, giving large clusters. On the other hand, SiO₂ has surface energy on the order of 4.32 J/m². Nickel tend to uniformly nucleate onto the SiO₂, resulting in continuous films. While the size of the resulting nickel clusters are comparable to metals grown on transferred graphene [32], it is much larger and more randomly distributed than most literature reported cluster growth on graphene in the form of moiré patterns [19-23]. This could be attributed to the amorphous SiO₂ substrate and other extrinsic factors (such as minor residue leftover) during graphene transfer process. Nonetheless, the resulting coalescent clusters show charge transfer with the graphene scaffold, which is evidenced by Raman spectroscopy (Figure 4). Consistent with recent literature [31], the fwhm (full width half maximum) of

the G band is broadened and the corresponding peak position is downshifted after nickel deposition. This is presumably due to the weakening of the graphene C-C bonds by the hybridization effect between the nickel d orbital and graphene p orbital at the interface. This could be further evidenced by the downshift of the 2D band shown in Figure 4b.

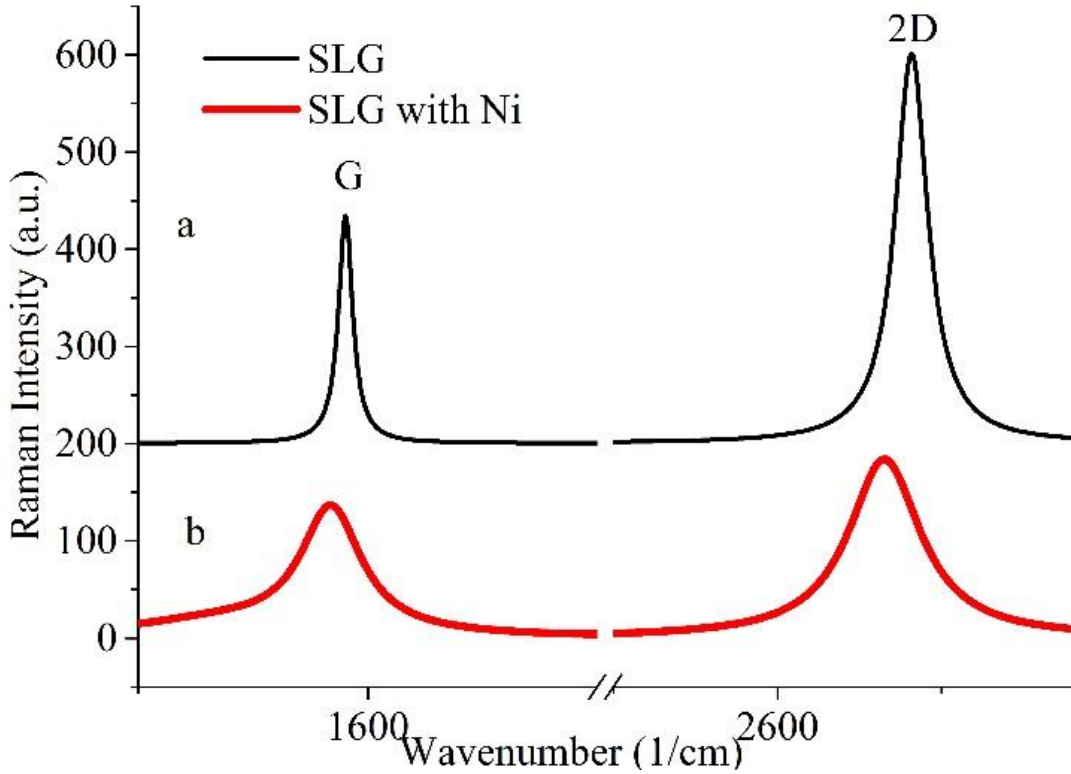


Figure 4. (Color online) Raman spectra of graphene: a) as-transferred, b) decorated with nickel cluster.

To further understand the graphene hybridized nickel-NiO_x system, exchange bias measurements were used to detect the changes before and after high vacuum annealing. Figure 5 shows the hysteresis loops (25 °C) before and after high vacuum annealing at 600 °C. Before high vacuum annealing, the hysteresis loop exhibits horizontal shifts, a strong indication that antiferromagnetic nickel oxide is pinning the ferromagnetic moment from metallic nickel. After the sample is annealed in high vacuum at 600 °C for 1 hr, the

asymmetry of the hysteresis loop is significantly reduced. This is consistent with a significant amount of reduction of nickel oxide as observed from the XPS analysis. With little presence of oxide, the exchange bias effect is dominated by nickel nanoclusters. Interestingly, it is worth noting that there are increases not only in zero field remanence for the annealed sample, but also in the coercive magnetization field for the same sample. The slightly increase in zero field remanence can be attributed to the reduction of antiferromagnetic nickel oxide, resulting in weight gain of ferromagnetic nickel. A similar observation was reported for nickel/nickel oxide on multilayer graphene nanosheet, in which ferromagnetic nickel showed high zero field remanence [33]. There are multiple factors that might contribute to the change in the coercivity, including particle size, shape, crystallinity and exchange anisotropy [34]. The impact of which one is dominant in a specific system is controversial and not well understood [35][36]. According to an idealized Meiklejohn-Bean theory, coercivity (H_c) is inversely proportional to the saturation magnification field (M_s) and proportional to the volume anisotropy constant (K_F) for the ferromagnetic materials [35]. With a small change in M_s in our specific case, the increase in H_c is related to K_F change. The details of which factors dictate the observed phenomenon will be a subject of future study. Nonetheless, it is worth mention that a similar H_c increase was seen on a control sample (Ni/SiO_2) with a much small magnitude.

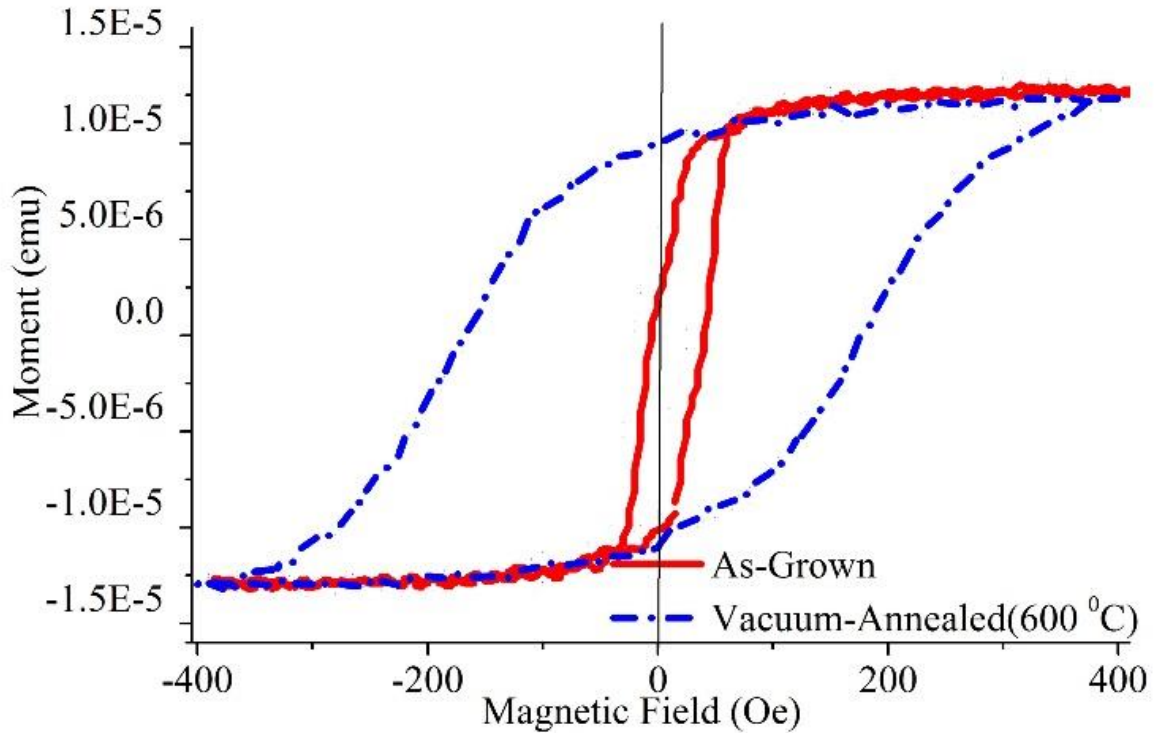


Figure 5. (Color online) Hysteresis loops (300 K) of nickel clusters: (1) as-grown (solid curve), (2) 600 °C annealed (dotted curve).

4. Conclusions

In summary, we demonstrate a simple method to hybridize randomly oriented nickel clusters with CVD graphene on SiO₂ substrate. The post fabrication oxidation effect of the nickel clusters was investigated and an alternative pathway to effectively reduce oxide using high vacuum annealing is suggested. The vacuum annealed nickel cluster is proved to be stable after air exposure. The findings provide a pathway to assemble metal cluster on high quality CVD graphene on an arbitrary substrate. The nickel clusters on electronically conductive graphene after vacuum annealing showed improved coercivity, which can be further explored as a building blocks for functional magnetic composite materials [37].

Acknowledgments

The authors acknowledge helpful discussion with Professor Carl Ventrice and the support from College of Nanoscience and Engineering at SUNY Polytechnic Institute.

References

- [1] de Heer WA (1993) The physics of simple metal clusters: experimental aspects and simple models. *Rev Mod Phys* 65: 611-676
- [2] McBain SC, Yiu HH, Dobson J (2008) Magnetic nanoparticles for gene and drug delivery. *Int J Nanomedicine* 3:169-180
- [3] Aiken JD, Finke RG (1999) A review of modern transition-metal nanoclusters: their synthesis, characterization, and applications in catalysis. *J Mol Catal A: Chem* 145: 1-44
- [4] Seo WS, Lee JH, Sun X, Suzuki Y, Mann D, Liu Z, Terashima M, Yang PC, McConnell MV, Nishimura DG, Dai H (2006) FeCo/graphitic-shell nanocrystals as advanced magnetic-resonance-imaging and near-infrared agents. *Nat Mater* 5: 971-976
- [5] Ishikawa FN, Stauffer B, Caron DA, Zhou C (2009) Rapid and label-free cell detection by metal-cluster-decorated carbon nanotube biosensors. *Biosens Bioelectron* 24: 2967-2972
- [6] Feyngenson M, Kou A, Kreno LE, Tiano AL, Patete JM, Zhang F, Kim MS, Solovyov V, Wong SS, Aronson MC (2010) Properties of highly crystalline NiO and Ni nanoparticles prepared by high-temperature oxidation and reduction. *Phys Rev B* 81: 014420-014428

- [7] Alonso F, Calvino JJ, Osante I, Yus M (2005) A new straightforward and mild preparation of nickel (0) nanoparticles. *Chem Lett* 34: 1262-1263.
- [8] Alonso F, Calvino JJ, Osante I, Yus M. (2006) Preparation of nickel (0) nanoparticles by arene-catalysed reduction of different nickel chloride-containing systems. *J Exp Nanosci* 1: 419-433.
- [9] Biswas A, Márton Z, Kanzow J, Kruse J, Zaporojtchenko V, Faupel F, Strunskus T (2003) Controlled generation of Ni nanoparticles in the capping layers of Teflon AF by vapor-phase tandem evaporation. *Nano Lett* 3: 69-73.
- [10] Zach MP, Penner RM (2000) Nanocrystalline nickel nanoparticles. *Adv Mater* 12: 878-883.
- [11] Novoselov KS, Geim AK, Morozov SV, Jiang D, Zhang Y, Dubonos SV, Grigorieva IV, Firsov AA (2004) Electric field effect in atomically thin carbon films. *Science* 306: 666-669.
- [12] Yazyev OV (2010) Emergence of magnetism in graphene materials and nanostructures. *Rep Prog Phys* 73: 056501- 056516
- [13] Wu ZS, Ren W, Wen L, Gao L, Zhao J, Chen Z, Zhou G, Li F, Cheng HM (2010) Graphene anchored with Co₃O₄ nanoparticles as anode of lithium ion batteries with enhanced reversible capacity and cyclic performance. *ACS Nano* 4: 3187-3194
- [14] Wang H, Robinson JT, Diankov G, Dai H (2010) Nanocrystal growth on graphene with various degrees of oxidation. *J Am Chem Soc* 132: 3270-3271
- [15] Simon P, Gogotsi Y (2008) Materials for electrochemical capacitors. *Nat Mater* 7: 845-854

- [16] Kamat PV (2009) Graphene-based nanoarchitectures. Anchoring semiconductor and metal nanoparticles on a two-dimensional carbon support. *J Phys Chem Lett* 1: 520-527
- [17] Hou J, Shao Y, Ellis MW, Moore RB, Yi B (2011) Graphene-based electrochemical energy conversion and storage: fuel cells, supercapacitors and lithium ion batteries. *Phys Chem Chem Phys* 13: 15384-15402
- [18] Matsubayashi A, Abel J, Sinha DP, Lee JU, LaBella VP (2013) Characterization of metal oxide layers grown on CVD graphene. *J Vac Sci Technol, A* 31: 021506-021514
- [19] Gerber T, Busse C, Mysliveček J, Coraux J, Michely T (2009) A versatile fabrication method for cluster superlattices. *New J Phys* 11: 103045-103063
- [20] N'Diaye AT, Bleikamp S, Feibelman PJ, Michely T (2006) Two-dimensional Ir cluster lattice on a graphene moiré on Ir (111). *Phys Rev Lett* 97: 215501-215504
- [21] Pan Y, Gao M, Huang L, Liu F, Gao HJ (2009). Directed self-assembly of monodispersed platinum nanoclusters on graphene moiré template. *Appl Phys Lett* 95: 093106-093108
- [22] Donner K, Jakob P (2009) Structural properties and site specific interactions of Pt with the graphene/Ru (0001) moiré overlayer. *J Chem Phys* 131: 164701-164710
- [23] Sicot M, Bouvron S, Zander O, Rüdiger U, Dedkov YS, Fonin M (2010) Nucleation and growth of nickel nanoclusters on graphene Moiré on Rh (111). *Appl Phys Lett*: 093115-093117
- [24] Alonso F, Riente P, Sirvent JA, Yus M (2010) Nickel nanoparticles in hydrogen-transfer reductions: characterisation and nature of the catalyst. *Appl Catal A: Gen* 378: 42-

- [25] Del Bianco L, Boscherini F, Tamisari M, Spizzo F, Antisari MV, Piscopiello E (2008) Exchange bias and interface structure in the Ni/NiO nanogranular system. *J Phys D: Appl Phys* 41: 134008-1314
- [26] Skumryev V, Stoyanov S, Zhang Y, Hadjipanayis G, Givord D, Nogues J (2003) Beating the superparamagnetic limit with exchange bias. *Nature* 423: 850-853
- [27] Antón RL, González JA, Andrés JP, Canales-Vázquez J, De Toro JA, Riveiro JM (2014) High-vacuum annealing reduction of Co/CoO nanoparticles. *Nanotechnology* 25: 105702-105709.
- [28] Grosvenor AP, Biesinger MC, Smart RS, McIntyre NS (2006) New interpretations of XPS spectra of nickel metal and oxides. *Surface Science* 600: 1771-1779
- [29] Cochran SJ, Larkins FP (1985) Surface reduction of some transition-metal oxides. An X-ray photoelectron spectroscopic study of iron, cobalt, nickel and zinc oxides. *J Chem Soc, Faraday Trans*, 81: 2179-2190.
- [30] Skriver H LK, Rosengaard N (1992) Surface energy and work function of elemental metals. *Phys Rev B*, 46, 7157
- [31] Hsu AL, Koch RJ, Ong MT, Fang W, Hofmann M, Kim K, Seyller T, Dresselhaus MS, Reed, EJ, Kong J, Palacios T (2014) Surface-induced hybridization between graphene and titanium. *ACS nano* 8: 7704-7713
- [32] Leong WS, Gong H, Thong JT (2013) Low-contact-resistance Graphene devices with Nickel-etched-Graphene contacts. *ACS nano*, 8: 994-1001.
- [33] Pawar SP, Stephen S, Bose S, Mittal V (2015) Tailored electrical conductivity, electromagnetic shielding and thermal transport in polymeric blends with graphene sheets decorated with nickel nanoparticles. *Phys Chem Chem Phys*, 17 : 14922-14930.

[34] Cullity BD, Graham CD, Introduction to magnetic materials. second ed., Hoboken, New Jersey, 2011.

[35] Radu F, Zabel H, Exchange bias effect of ferro-/antiferromagnetic heterostructures. Magnetic heterostructures, Springer: 2008, pp 97-184.

[36] Hwang JH, Dravid V, Teng M, Host J, Elliott B, Johnson D, Mason T(1997) Magnetic properties of graphitically encapsulated nickel nanocrystals. J Mater Res, 12: 1076-1082.

[37] Lu AH, Salabas EeL, Sch üth F (2007) Magnetic nanoparticles: synthesis, protection, functionalization, and application. Angew Chem Int Ed, 46: 1222-1244.